Image Quality Error Budgets for the Giant Magellan Telescope

Breann Sitarski*[a], Antonin Bouchez[a], Rodolphe Conan[a], Marcos van Dam[b], Fernando Quirós-Pacheco[a], George Angeli[a], Brian McLeod[c]
[a]Giant Magellan Telescope Organization, 465 N. Halstead St., Pasadena, CA 91107, USA;
[b]Flat Wavefronts, P.O. Box 1060, Christchurch 8140, New Zealand;
[c]Smithsonian Astrophysical Observatory, 60 Garden St., Cambridge, MA 02138, USA;

ABSTRACT

Image Quality is one of the key performance parameters for the Giant Magellan Telescope (GMT). The image quality requirements are derived from the top-level Science Requirements Document (SRD) for each data type and flowed down to the Observatory Requirements Document (ORD) to Normalized Point Source Sensitivity (PSSN) or RMS wavefront error for different wavefront control modes (natural seeing [NS], ground layer adaptive optics [GLAO], laser tomography adaptive optics [LTAO], and natural guide star adaptive optics [NGAO]). The values are further broken down and distributed to error terms on the subsystems in the level three Observatory Architecture Document (OAD) for each of the data types and wavefront control modes (observing performance modes). The primary contributor terms to each error budget includes thermal, optical design, segment shape, segment alignment, and tracking and vibration errors for NS modes; all AO modes have additional turbulence correction and AO calibration errors.

We present the current image quality budgets for all wavefront control modes and observatory configurations for the GMT, expressed either in PSSN (NS and GLAO) or nm RMS wavefront error (LTAO and NGAO). A breakdown of the largest error terms along with preliminary mitigation strategies is presented. Updates and reviews of the error budget will continue to be done on a regular basis with involvement and communication with each of the subsystems of GMT.

Keywords: Image quality, extremely large telescopes, adaptive optics, active optics,

1. INTRODUCTION

The 25.4-meter Giant Magellan Telescope (GMT) is part of the next generation of extremely large telescopes (ELTs) that are set to have first light within the next decade. It will be located at Las Campanas Peak, one of the best natural seeing sites in the world with a median seeing of 0.63 arcseconds in the V-band. The primary aperture has an aplanatic Gregorian design, which is useful for canceling low-order aberrations. The entrance aperture consists of seven 8.4-meter diameter segments that are perfectly conjugated to 7 segmented, 1.05-meter secondary mirror segments. Two secondary mirrors are currently planned: a fully adaptive secondary mirror conjugated to the ground layer of the atmosphere to facilitate excellent Ground Layer Adaptive Optics correction and will be used for Natural Guide Star and Laser Tomographic Adaptive Optics, and a fast-steering secondary mirror that will allow for piston, tip, and tilt for natural seeing modes when the adaptive secondary is undergoing maintenance. The optical design of GMT enables large fields of view (up to 20 arcminutes in diameter), and its compact f/8 focus gives a ~1 arcsecond/mm plate scale that equates to fairly compact instruments for an ELT. For more information about GMT, see Fanson et al. (2018)[1].

Image quality is one of the key metrics for defining the performance of the GMT during commissioning and beyond. The image quality requirements are derived from the top-level Science Requirements Document (SRD[2]; level 1) and Concept of Operations Document (ConOps[3]; level 1) and flowed down to the Observatory Requirements Document (ORD[4]; level 2). Natural seeing and GLAO requirements are converted from FWHM to Normalized Point Source Sensitivity (PSSN) at level 2; NGAO and LTAO requirements are converted to RMS wavefront error. The level 2 value denotes the minimum image quality that the GMT must deliver over various fields of view, environmental conditions, and regions of the sky. These level 2 values are then flowed down to level 3 budgets in the Observatory Architecture Document (OAD[5]) where allocations are given to each component of the telescope based on simulations and analysis. Further flow-down to level 4 and below is facilitated via additional simulations.

*bsitarski@gmto.org; phone 1 626 204-0500 x 5233; http://gmto.org

The natural seeing mode delivers images that are only limited by the naturally-occurring optical turbulence of the site. Gravitational and thermal distortion of the structure and optics, tracking errors, and wind shake are corrected by active optics as they are slowly varying effects (i.e., Conan et al. 2016[6], Conan et al. 2018[7]). Dome seeing is not corrected, as it is rapidly changing. The GLAO mode has many of the same terms as the natural seeing image quality budget, but there is some improvement in image quality due to the higher spatial and temporal wavefront control bandwidth of the system using the adaptive secondary mirror. Quickly varying terms, including atmospheric and dome seeing terms, can be at least partially corrected in GLAO mode. The natural guide star AO mode uses a single bright, on-axis natural guide star and a single natural guide star wavefront sensor ahead of the instrument to provide atmospheric turbulence information to the adaptive secondary mirror to achieve diffraction-limited performance over a small field of view in the near-infrared. The laser tomography AO mode uses an asterism of 6 laser guide stars to reconstruct high-order components of atmospheric turbulence towards the science target. A natural guide star tracks tip, tilt, focus, and dynamic calibration terms, while the active optics system uses four other stars to ensure that the telescope is phased. For more information, see Bouchez et al (this conference)[8].

The image quality error budgets at level 3 are established using preliminary analyses and designs with some margin. The analyses are often based on existing requirements and/or as-built measurements (i.e., polishing error). The allocations are the flowed-down to level 4 requirements on engineering terms (i.e., hardpoint repeatability).

1.1 Environmental Conditions

Image quality is a statistical quantity and is defined in median conditions for the GMT error budgets. The median conditions at the site are given in **Table 1** below. Reference values for the FWHM are given in **Table 2**, and the optical atmospheric turbulence profile (Goodwin 2009[9]) is given in **Table 3**.

Table 1: Reference Environmental Conditions

Parameter	**Condition**	**Reference**
Zenith angle (φ)	30°	Magellan telescopes' median observing condition
Cloud opacity	photometric	GMT site nighttime condition ~60% of the time
Wind speed (v_w)	6.3 m/s	GMT site nighttime median wind
Wind azimuth (θ_w)	31.6°	GMT site median value 12 m above grade
Temperature (T)	11.6°C	GMT site nighttime median
Temperature rate of change (dT/dt)	0.7°C/hour	GMT site 1σ value of 30 minute average
Relative humidity (H_R)	36%	GMT site nighttime median
Fried parameter at zenith (r_0)	0.160 m	GMT site nighttime median
Turbulence outer scale (L_0)	25 m	La Silla nighttime median
AO time constant (τ_0)	2.6 ms	GMT site nighttime median

Table 2: Reference PSF Parameters

Parameter	**0.5 µm**	**1.65 µm**
FWHM	505 mas	314 mas

Table 3: Optical Atmospheric Turbulence Profile (Goodwin 2009[9])

Height (m)	**25**	**275**	**425**	**1250**	**4000**	**8000**	**13000**
Uncorrected C_n^2 (10^{-13} $m^{-1/3}$)	0.440	0.304	0.234	1.223	0.794	0.238	0.262
Ideal GLAO C_n^2 (10^{-13} $m^{-1/3}$)	0.031	0.017	0.025	0.367	0.508	0.200	0.246
Wind Speed (m/s)	5.65	5.80	5.89	6.64	13.29	34.83	29.42

Wind Direction (°)	0.78	8.25	12.48	32.50	72.10	93.20	100.05

1.2 Normalized Point Source Sensitivity

The natural seeing and GLAO image quality error budgets are expressed in terms of the normalized point source sensitivity (PSSN; Seo et al. 2009[10]; Angeli et al. 2011[11]). PSSN relates the actual performance of the system to a reference, typically the equivalent noise area (ENA) of the representative atmosphere of the site with a perfect telescope. The PSSN is given by:

$$PSSN = \frac{\iint |PSF_{a+t+e}|^2}{\iint |PSF_{a+t}|^2}$$

where PSF_{a+t+e} is the time-averaged PSF of the atmosphere and aberrated telescope while PSF_{a+t} is the time-averaged PSF of the atmosphere and perfect telescope. PSSN is multiplicative.

GLAO correction reduces the ENA by correcting some of the ground-layer turbulence. Maintaining the same uncorrected atmosphere as a reference would yield PSSNs larger than one; we instead reference the atmospheric wavefront error after correction by an ideal GLAO system with a single deformable mirror at the conjugate height of M2.

For most of the error terms, the PSSN is computed using optical transfer functions (OTFs). Three OTFs are computed: the optical turbulence OTF, the OTF of a perfectly-aligned GMT, and the OTF of the telescope with aberrations that induce image quality errors. The optical turbulence OTF is computed via analytical expressions for the long-exposure von Karman turbulence. The telescope OTFs are computed with Cuda Engined Optics (CEO).

2. NATURAL SEEING AND GROUND LAYER ADAPTIVE OPTICS IMAGE QUALITY ERROR BUDGETS

The tabulated natural seeing and GLAO image quality error budgets for the GMT are given in Table 4 below. Each blue row denotes an overall "theme" of an error, while the lines below show the breakdown of that theme. An example is given for M1 segment shape in Section 2.2.

Table 4: Natural Seeing and GLAO Image Quality Error Budget

Direct Gregorian Narrow Field	On-Axis Image Quality		Average IQ over 10' FOV		
Error Term	Natural Seeing		GLAO		Description
	0.5 µm	**1.65 µm**	**0.5 µm**	**1.65 µm**	
Thermal	**0.9394**	**0.9594**	**0.9666**	**0.9692**	
Dome Seeing	0.9405	0.9624	0.9681	0.9740	Optical turbulence from Enclosure, Mount, Equipment
Mirror Seeing	0.9988	0.9969	0.9985	0.9951	Optical turbulence at M1 and M2
Optical Design	**1.0000**	**0.9989**	**0.9960**	**0.9940**	
Design Aberrations	1.0000	1.0000	1.0000	1.0000	Telescope design aberrations on-axis
Segment Phasing	1.0000	0.9989	0.9960	0.9940	Error due to uncontrolled segment phase piston
Segment Shape	**0.9157**	**0.9468**	**0.9217**	**0.9496**	
M1 Segment Shape	0.9295	0.9669	0.9247	0.9559	M1 segment shape errors after Active Optics Correction
M2 Segment Shape	0.9883	0.9852	0.9990	0.9980	M2 segment shape errors
AGWS Shape Measurement	0.9967	0.9939	0.9977	0.9954	Shape errors due to AGWS measurement and estimation
Segment Alignment	**0.9905**	**0.9794**	**0.9925**	**0.9834**	

M1 Segment Position	0.9995	0.9976	1.0000	1.0000	M1 segment positioner repeatability
M2 Segment Position	0.9975	0.9932	1.0000	1.0000	M2 segment positioner repeatability
Instrument Position	0.9995	0.9992	0.9994	0.9987	Instrument displacement with respect to reference focal plane
AGWS Alignment	0.9968	0.9931	0.9966	0.9907	Alignment errors due to AGWS measurement and estimation
SWC DAR	0.9980	0.9972	0.9975	0.9956	Error in differential atmospheric refraction correction
Instrument Sensor	0.9992	0.9989	0.9990	0.9983	Instrument flexure sensor tip-tilt and focus error
Dynamic Optical Alignment	**0.9734**	**0.9544**	**0.9685**	**0.9360**	
Dynamic Control	0.9830	0.9735	0.9805	0.9657	Image motion and blur caused by control loops
Wind Residual	0.9958	0.9914	0.9947	0.9865	Wind image motion and blur after tip-tilt correction
Vibration Residual	0.9944	0.9888	0.9930	0.9825	Vibration image motion and blur after tip-tilt correction
Turbulence Correction	**1.0030**	**1.0090**	**--**	**--**	
Segment Tip-Tilt	1.0030	1.0090	--	--	IQ improvement due to global & segment tip-tilt correction
GLAO Errors	**--**	**--**	**0.8488**	**0.8457**	
Guide Stars + Fitting Error	--	--	0.8528	0.8558	Error due to guide star number, location, and WFS sampling
AGWS Measurement	--	--	0.9987	0.9968	Physical optics, detector noise, photon noise, and background
AGWS Latency	--	--	0.9966	0.9914	Latency error, dominated by ≥88 Hz readout rate specification
TOTAL:	**0.8318**	**0.8557**	**0.7240**	**0.7121**	Product of above bolded terms
REQUIREMENT:	**0.8258**	**0.7888**	**0.6839**	**0.5638**	Flow-down from Observatory Requirements Document
Margin:	**3.45%**	**31.70%**	**12.68%**	**34.01%**	Ratio of (1-PSSN)

2.1 Dome Seeing

Dome seeing is caused by thermal turbulences and imbalances within the enclosure. It is a rapidly varying phenomenon that is caused by mix convection of thermally inhomogeneous ambient air by the enclosure and the mount. Dome seeing limits the performance of large telescopes in the natural seeing wavefront control mode, and inadequate flushing of the dome will result in degraded performance.

In an effort to understand dome seeing, GMT has developed computational fluid dynamics (CFD) simulations that are run at various telescope-to-wind direction azimuths and wind speeds (see Conan et al. [this conference][12]). Changes in the refractive index are ray-traced to the telescope exit pupil and optical path differences are obtained and converted into PSSN. The simulations are used in conjunction with the Standard Year framework (see Sitarski et al. [this conference][13]) to determine the median-condition PSSN. An example of the refractive index gradient along the midplane of the enclosure via the dome-seeing CFD simulations is shown on the left-hand side of **Figure 1**. The right-hand side shows the OPD map at the telescope exit pupil at the same timestep.

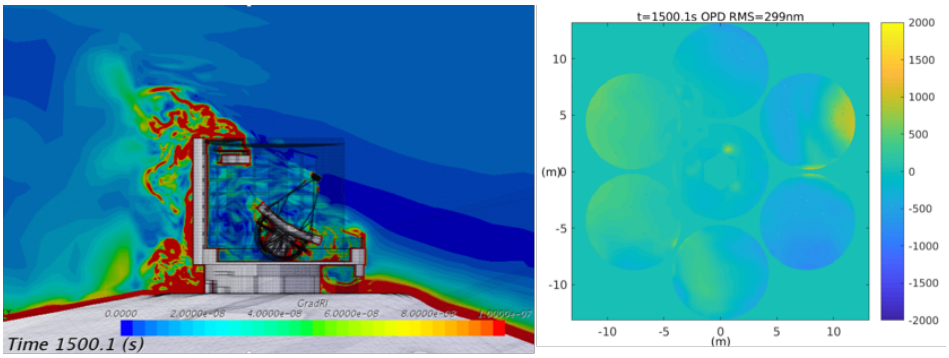

Figure 1: Refractive index gradient of the enclosure (left) and corresponding OPD at the telescope exit pupil.

2.2 M1 Segment Shape Errors

M1 segment shape errors describe the image quality degradation due to residual shape errors of the primary mirror after correction by the active optics system. A breakdown of the M1 segment shape errors are shown in Figure 2 with PSSN allocations for the natural seeing image quality budget.

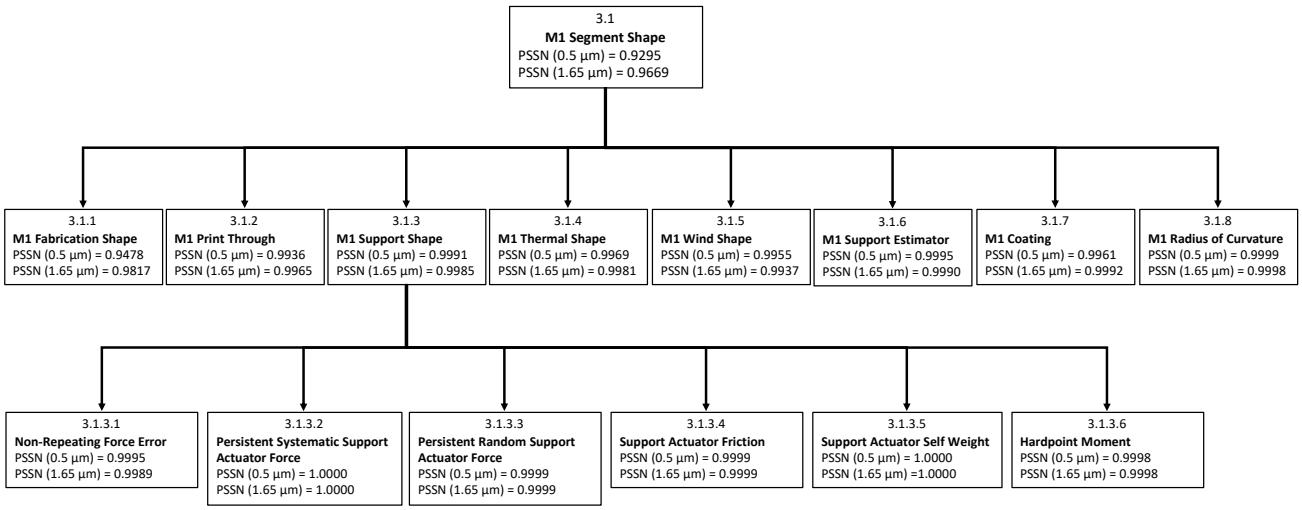

Figure 2: M1 segment shape error flow-down example in the natural seeing wavefront control mode.

Each individual term in Figure 2 is flowed-down to engineering terms and requirements on individual pieces of hardware. For example, the M1 Fabrication Shape term refers to static polishing errors and flows-down to the polishing specifications given to the Richard F. Caris Mirror Lab at the University of Arizona in the form of a structure function (**Figure 3** left). As mirror segments are polished and the final specifications are determined, the polishing residuals are included in CEO to determine the effect on PSSN. We currently have two mirror cells fully accepted, and they meet our specification. The residual surface figure after correction by 27 bending modes from the active optics system is shown in **Figure 3** (right).

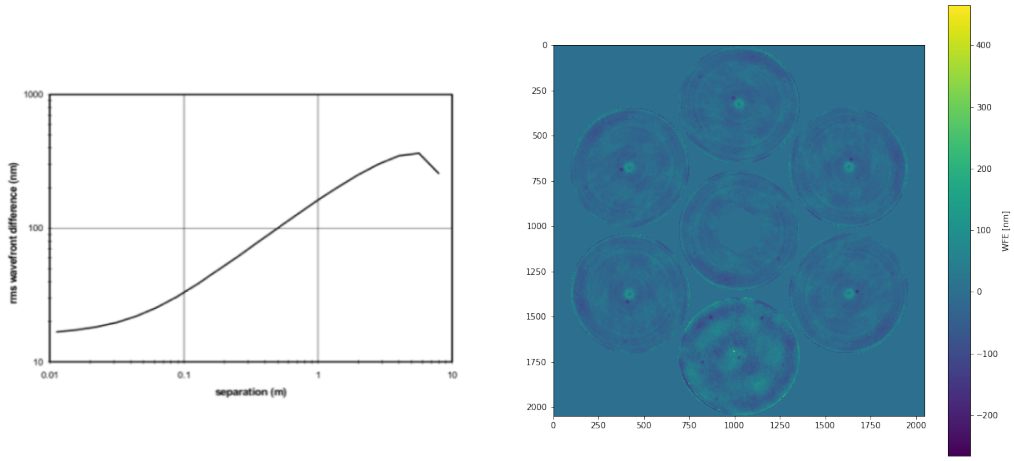

Figure 3: Figure 1: Left: Specification for clear aperture figure accuracy. Right: surface figure from polishing residuals with 1 x S1 and 6 x S2.

2.3 Turbulence Correction

Segment tip-tilt compensation describes the *improvement* in image quality arising from partial correction of atmospheric tip-tilt over the spatial scale of the M1 segments. The fast segment tip-tilt control loop corrects global and segment pointing error at a bandwidth of ~8 Hz and has the unintended consequence of correcting guiding errors and wind buffeting at high temporal frequencies. The value given in **Table 4** is the median improvement at 99% sky coverage.

Figure 4 shows resulting PSSN from the correction of segment tip-tilt using a bright off-axis guide star (the simulations do not include measurement latency or sensor error). The segment tip-tilt error due to latency is negligible compared to anisoplantism and is included in another term in the budget. The value given in **Table 4** was computed using guide stars at a 6.5' field angle.

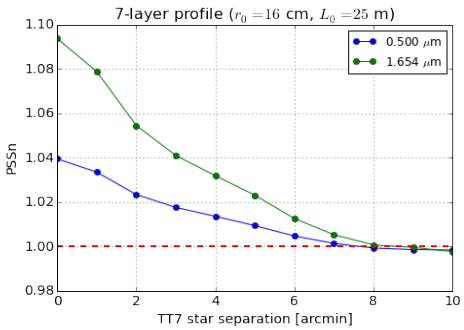

Figure 4: Resulting PSSN from correction of segment tip-tilt using a bright off-axis guide star.

2.4 GLAO: Guide Stars and Fitting Error

Many of the error terms in the GLAO image quality error budget are derived using the median asterism at the South Galactic Pole, shown in **Figure 5**. The median asterism was selected by simulating star fields for the South Galactic Pole using the Besancon star model. Asterisms are ranked in terms of expected performance by evaluating the sum of the tomographic reconstruction and measurement noise errors, and the median case was chosen for GLAO simulations. More information about construction of this asterism and the application of the asterism can be found in van Dam et al (2014)[14]. The error term here describes the error induced from asterism variation.

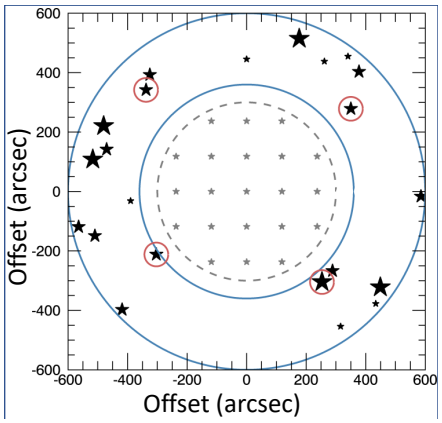

Figure 5: Median asterism at the South Galactic Pole

3. NATURAL GUIDE STAR ADAPTIVE OPTICS AND LASER TOMOGRAPHY ADAPTIVE OPTICS ERROR BUDGETS

For the high-resolution observing cases, GMT will use NGAO (high-contrast imaging) and LTAO (diffraction-limited observations at 50% and 80% sky coverages). The two error budgets are developed in terms of wavefront error RMS and includes different terms for each of the AO modes. Each of the terms are flowed-down to requirements on the subsystem, including the adaptive secondary mirror (i.e., dynamic range of motion budget) and the mount structure (i.e., vibration).

The values given in Table 5 represent the amount of wavefront error coming from image blur and image motion form low- and high-order aberrations. For tip-tilt error, 1 mas of error is equivalent to 29.8 nm RMS of wavefront error.

Table 5: LTAO and NGAO Image Quality Error Budgets Breakdown

Error Term	On-Axis WFE (nm RMS) at 1.65 μm			Description
	NGAO	LTAO (50% SC)	LTAO (80% SC)	
	CBE (r_0 = 16cm)			
Thermal	**19.1**	**28.8**	**28.8**	
Dome Seeing	18.8	28.2	28.2	Optical turbulence from Enclosure, Mount, Equipment
Mirror Seeing	3.2	5.9	5.9	Optical turbulence at M1 and M2
Optical Design & Phasing	**46.9**	**84**	**86**	
Design Aberrations	0	0	0	Telescope design aberrations on-axis
Segment Phasing	46.9	84	86	Error due to uncontrolled segment phase piston
Segment Shape & Alignment	**32**	**32**	**32**	
M1 Segment Shape	15	15	15	M1 segment shape errors after AcO correction
M2 Segment Shape	28.3	28.3	28.3	M2 segment shape errors
M1 Segment Position	0	--	--	M1 segment positioner precision
M2 Segment Position	0	--	--	M2 segment positioner precision
Instrument Position	0	--	--	Instrument displacement relative to focal plane
Tracking & Vibration	**45.3**	**172**	**249.2**	
Dynamic Control	11.2	33.5	33.5	Image motion and blur caused by telescope control loops
Wind Residual	30	73.4	73.7	Wind image motion and blur after tip-tilt correction

Vibration Residual	30.8	46.2	46.2	Vibration image motion and blur after tip-tilt correction
Instrument OIWFS	6.2	144.5	231	Instrument image motion and focus sensing error
SWC DAR	6.2	6.2	6.2	Error in differential atmospheric refraction correction
Turbulence Correction	**85**	**156.3**	**163.9**	
ASM Errors	70.5	70.5	70.5	ASM fitting, temporal, and repeatability errors
NGWS Errors	47.5	--	--	NGWS measurement and temporal errors
LTWS Errors	--	74.3	74.3	LTWS fitting, measurement, and temporal errors
Instrument OIWFS	--	35.1	60.6	Instrument OIWFS truth-sensing errors
OCS Latency	0.8	1.7	1.7	OCS computation and communication errors
Tomography	--	112.7	112.7	On-axis tomographic error
Anisoplanatism	--	0	0	Angle between guide star and science target
AO Calibration	**75.7**	**85.7**	**85.7**	
ASM/System Calibration	50	50	50	ASM-NGWS/NGWS interaction matrix, control models, etc.
NGWS Calibration	30	--	--	Pyramid optical errors, pupil mapping errors
LTWS Calibration	--	30	30	Error in reference slopes, pupil size/distortion
Instrument OIWFS Calibration	30	30	30	Truth sensor optical errors
Residual NCPA	28.3	49.2	49.2	NCPA errors after calibration & truth sensor correction
Pupil Alignment	25	25	25	Dynamic Pupil alignment errors on NGWS and Truth WFS
TOTAL	**136.3**	**265.1**	**324.9**	RSS of above bolded terms
Requirement	**150**	**280**	**350**	Flow-down from the Observatory Requirements Document
Margin	**70**	**90**	**130**	SQRT(Requirement^2 - Total^2)

3.1 Segment Phase Piston Errors

One clear discrepancy between the LTAO and NGAO errors is segment phase piston. M1 and M2 edge sensors are critical for the TLAO mode that measure high temporal frequency segment phase piston errors (f_{ES} = 200 – 500 Hz). Edge sensors will have some long-term drifts from gravitational and thermal effects. This error is mitigated in NGAO mode with the natural guide star wavefront sensor that measures low and high temporal frequency segment phase piston errors ($f_{pyramid}$ = 1 kHz). Figure 6 below shows the residual segment phase piston power spectral density plot with and without LTAO. This was computed from a model that was developed to determine the phasing strategy and the influence of wind buffeting on phasing errors in LTAO mode (Quirós-Pacheco et al. 2018[15]).

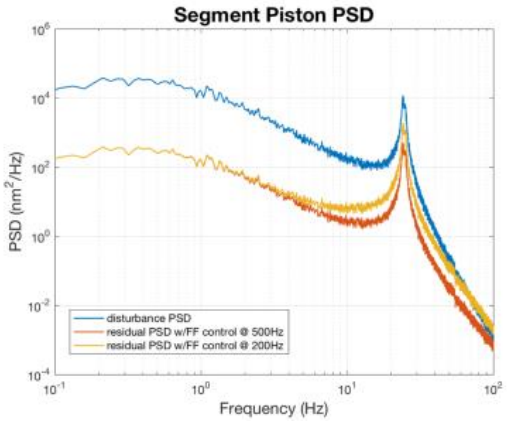

Figure 6: Residual segment phase piston from wind buffeting in LTAO line. The blue line denotes the segment phase piston error with active optics feedback. The yellow line denotes the residuals in the LTAO mode with feed-forward at 200 Hz and (blue) at 500 Hz.

3.2 Tracking and Vibration Errors

The largest tracking and vibration discrepancies come from using a large asterism and field-dependent errors in LTAO mode. The tip-tilt anisoplanatism (anisokinetism) is estimated using a 30 arcsecond off-axis guide star. Median values are computed for the error based on random occurrence of atmospheric phase screens that are all based on the same atmospheric parameters. The median condition WFE is 111 nm/200 nm for the 50%/80% sky coverage LTAO cases with a natural guide stars 30"/60" off-axis. A single occurrence from the distribution is shown in **Figure 7** below.

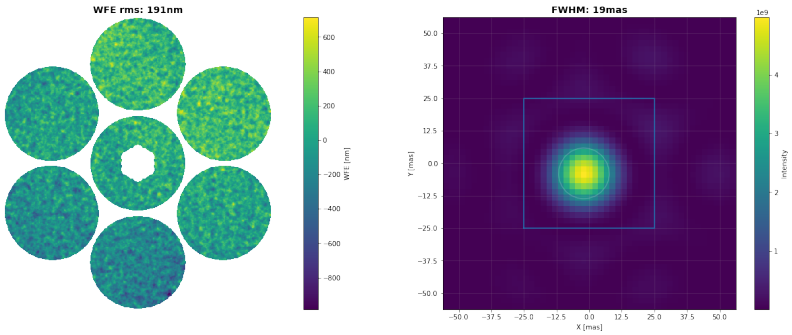

Figure 7: Anisokinetism error estimated with a 30" off-axis guide star.

3.3 NGWS and LTWS Errors

The natural guide star wavefront sensor (NGWS) senses, at high frequencies (1 kHz) wavefront aberrations from the telescope and atmosphere with high sensitivity and low noise levels (Bouchez et al. 2018). The NGWS errors given in Table 5 are composed of measurement, aliasing, and temporal errors that describe characteristics of the camera (including temporal effects and assuming that exposures are taken at a 1 kHz frequency) and effects of aliasing of high spatial frequencies into measurements of small correctable spatial frequencies. Error terms for the NGWS were determined via an analysis for an R = 10 guide star at 1 kHz, 1 electron RMS of readout noise, sqrt(2) EMCCD noise, a total throughput (including quantum efficiency) of 0.26, a $\pm 2\lambda/D$ modulation on the pyramid wavefront sensor, and an additional piston measurement error of 10 nm. The temporal error is based on 1500 microseconds of latency. For more information on the NGAO simulations, please see Pinna et al. 2014[16].

The laser tomography wavefront sensor (LTWS) provides high-order wavefront sensing at ~500 Hz for the GMT diffraction-limited modes. LTWS errors arise from error in atmospheric fitting, sensor measurement noise, aliasing, and latency errors (assuming 3.0 ms of latency). The allocations in the budget were derived from a series of LTAO simulations that assume 6 evenly-arranged laser guide stars arranged on a 30 arcsecond radius scale; each LGS has a 60 x 60 Shack-

Hartmann wavefront sensor that tracks the LGS asterism. For more information on the LTAO simulations and design, see Conan et al. (2012)[17] and van Dam et al. (2011)[18]. Figure 8 shows an example of the OPD of the combined tomographic and aliasing errors on the exit pupil and a recreation of the point spread function.

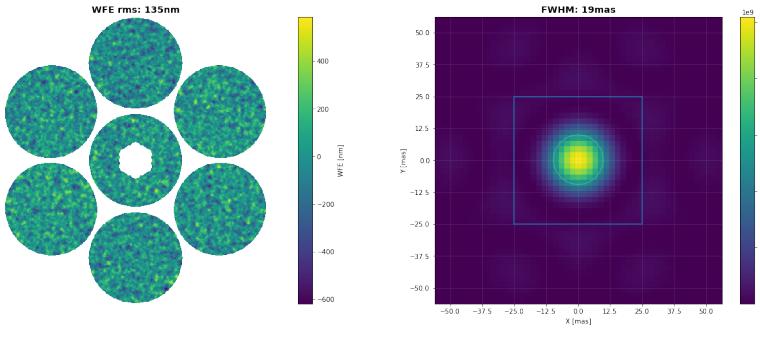

Figure 8: *Left*: OPD of the combined tomographic and aliasing errors at the exit pupil. *Right*: point spread function from OPD.

4. FUTURE WORK

While many of the allocations of the image quality budgets have been simulated, several still need to be developed and explored. Additionally, the natural seeing and GLAO image quality budgets are currently only defined for the direct Gregorian narrow field optical configuration (10' FOV), but both wavefront control modes can also be operated in the direct Gregorian wide field (DGWF) configuration. An initial budget for the natural seeing wavefront control mode in the DGWF configuration has been started but work should be completed. All adaptive optics modes will also be in the folded port (FP) configuration that includes a tertiary mirror; NGAO and LTAO budgets need to be adjusted to take the tertiary mirror into account. Other budgets that pertain to image quality, including image quality spatial variation and image quality temporal stability, will be computed as part of an effort to define the key performance parameters for GMT.

REFERENCES

[1] Fanson, J., McCarthy, P., Bernstein, R., Angeli, G., Ashby, D., Bigelow, B., Bouchez, A., Burgett, W., Chauvin, E., Contos, A., Figueroa, F., Gray, P., Groark, F., Laskin, R., Millan-Gabet, R., Rakich, A., Sandoval, R., Pi, M., Wheeler, N., "Overview and Status of the Giant Magellan Telescope project," Proc. SPIE 10700, Ground-Based and Airborne Telescopes VII, 1070012 (2018).
[2] https://www.gmto.org/wp-content/uploads/web-GMT-REQ-03213_Rev.-C_GMT-Science-Requirements-Document.pdf
[3] https://www.gmto.org/wp-content/uploads/web-GMT-DOC-03205_Rev.-B_GMT-Concept-of-Operations-Document.pdf
[4] https://www.gmto.org/wp-content/uploads/web-GMT-REQ-03214_Rev.-B_GMT-Observatory-Requirements-Document-ORD.pdf
[5] https://www.gmto.org/wp-content/uploads/web-GMT-REQ-03215_Rev.-B_GMT-Observatory-Architecture-Document-OAD.pdf
[6] Conan, R., Bouchez, A., Quiros-Pacheco, F., McLeod, B., Ashby, D., "The GMT active optics control strategies," Proc. SPIE 9909, Adaptive Optics Systems V, 99091T (2016).
[7] Conan, R., van Dam, M. A., Bouchez, A. H., Angeli, G. Z., Ashby, D., McLeod, B. A., Quiros-Pacheco, F., "Control algorithm and performance of the active optics systems of the Giant Magellan Telescope," Proc. SPIE 10700, Ground-based and Airborne Telescopes VII, 1070034 (2018).
[8] Bouchez, A. H., et al., "GMT Active and Adaptive Optics Overview," this conference.
[9] Goodwin, M. S., "Turbulence profiling at Siding Spring and Las Campanas Observatories," Ph.D. Thesis, Australian National University (2009).
[10] Seo, B.-J., Nissly, C., Troy, M., Angeli, G., "Analysis of normalized point source sensitivity as a performance metric for large telescopes," Applied Optics, 48, 31 (2009).

[11] Angeli, G. Z., Seo, B.-J., Nissly, C., Troy, M., “A convenient telescope performance metric for imaging through turbulence,” Proc. SPIE 8127, Optical Modeling and Performance Predictions V, 812709 (2011).
[12] Conan, R., et al., “Modeling the Giant Magellan Telescope dome seeing using fluid dynamics simulations,” This conference.
[13] Sitarski, B. N., Vogiatzis, K., Conan, R., Angeli, G. Z., Goodrich, B., “Performance Estimates for the Giant Magellan Telescope via Statistical Analysis,” this conference.
[14] van Dam, M., Bouchez, A., McLeod, B., “Wide field adaptive optics correction for the GMT using natural guide stars,” Proc SPIE 9148, Adaptive Optics Systems IV, 914813 (2014).
[15] Quirós-Pacheco, F., Schwartz, D., Das, K., Conan, R., Bouchez, A., Irarrazaval, B., McLeod, B, “The Giant Magellan Telescope phasing strategy and performance,” Proc. SPIE 10700, Ground-based and Airoborne Telescopes VII, 107000N (2018)
[16] Pinna, E., Agapito, G., Quirós-Pacheco, F., Antichi, J., Carbonaro, L., Briguglio, R., Bonaglia, M., Riccardi, A., Puglisi, A., Biliotti, V., Arcidiacono, C., Xompero, M., Di Rico, G., Valentini, A., Bouchez, A., Santoro, F., Trancho, G., Esposito, S., “Design and numerical simulations of the GMT Natural Guide Star WFS,” Proc. SPIE 9148, Adaptive Optics Systems IV, 91482M (2014).
[17] Conan, R., Bennet, F., Bouchez, A., van Dam, M., Espeland, B., Gardhouse, W., d’Orgeville, C., Parcell, S., Piatrou, P., Price, I., Rigaut, F., Tracho, G., Uhlendorf, K, “The Giant Magellan Telescope laser tomography adaptive optics system,” Proc. SPIE, Adaptive Optics Systems III, 84473P (2012).
[18] van Dam, M. A., Conan, R., Bouchez, A. H., Espeland, B., “Aberrations induced by side-projected laser guide stars in laser tomography adaptive optics systems,” Proc. AO4ELT2, 67 (2011).